Structural and optical properties of Si/SiO_2 superlattices prepared by low pressure chemical vapor deposition

Zhenrui Yu,[a] Mariano Aceves-Mijares, Enrique Quiroga, and R. Lopez-Estopier
Department of Electronics, INAOE, Apartado Postal 51, Puebla, Puebla 72000, Mexico

Jesus Carrillo
CIDS-ICUAP, Universidad Autónoma de Puebla, Apartado Postal 1651, Puebla, Puebla 72570, Mexico

Ciro Falcony
Department of Physics, CINVESTAV-IPN, Mexico Distrito Federal, Apartado Postal 14 740, 07000 Mexico

(Received 14 October 2005; accepted 3 May 2006; published online 13 July 2006)

Si/SiO_2 superlattices (SLs) structures were prepared using a low-pressure chemical vapor deposition (LPCVD) method. The structural and optical properties of the SLs materials were characterized using atomic force microscopy (AFM), Fourier transformed infrared (FTIR) absorption, x-ray diffraction, and room-temperature photoluminescence (PL) measurements. The AFM results show that a periodically layered Si/SiO_2 structure was successfully deposited with nanometer-sized Si dots embedded in the Si layers. The FTIR spectra show that the SiO_2 near the Si/SiO_2 interface is more ordered than the amorphous SiO_2 in the center of the SiO_2 layers. The Si/SiO_2 SLs films show a room-temperature PL in the visible-near infrared wavelength region. The PL intensity is significantly enhanced by a high-temperature annealing at 1100 °C. The peak position and intensity of the main emission band in the PL spectra strongly depend on the Si layer thickness. A pronounced redshift with increasing Si layer thickness is observed. This emission peak position can be fitted by the theory of quantum confinement effect in Si dots. The emission from recombination through defect and interface states was also observed in the SLs films. © *2006 American Institute of Physics*. [DOI: 10.1063/1.2210667]

I. INTRODUCTION

Silicon is a leading material in the microelectronic technology. With the continuous scaling down of the device size, the interconnection has become a bottleneck for further increase of the integration density and the integration level approaches its limit. To overcome the technique barrier, researchers have looked for new approaches by combining the photonic and electronic components on a single chip. Because of its indirect band gap of 1.12 eV, bulk silicon is generally a very poor optical emission material. However, a great deal of research on silicon nanocrystals (nc) embedded in silicon oxide matrix has been conducted recently and it has been shown that the thin films with nanometer scale silicon dots are efficient light-emission materials.[1–8] As an approach towards the nanocrystalline silicon materials, Si/SiO_2 double barrier (DB) structures and superlattices (SLs) have been studied and intensive light emissions have been observed.[9,10] There are evidences that the light emission from Si/SiO_2 DB structures or SLs is due to the quantum confinement effect in the Si dots.[9,10]

Si/SiO_2 SLs materials are usually prepared by molecular beam epitaxy (MBE),[9] magnetron sputtering,[11–13] epitaxial layers transfer (ELTRAN) technology,[10] and plasma enhanced chemical vapor deposition (PECVD).[13] Low pressure chemical vapor deposition (LPCVD) has never been used to prepare Si/SiO_2 SLs. LPCVD is a simple and convenient method for the deposition of Si and silicon oxide materials and is completely compatible with Si integrated circuit (IC) technology. Therefore, the research on the fabrication of Si/SiO_2 SLs using LPCVD and the analysis of the structural and optical properties becomes a significant important topic from the technology's point of view.

In this article, we report our recent results of Si/SiO_2 SLs films deposited using LPCVD. We demonstrate that LPCVD can be used for this application. The structural and optical properties of the Si/SiO_2 SL films were studied using various methods. We observed an intensive room-temperature photoluminescence (PL) and found that the PL intensity and peak position can be modified by changing the Si layer thickness and by thermally annealing at a high temperature.

II. EXPERIMENT

The nc-Si/SiO_2 SL samples were deposited using LPCVD. The SL films consisting of 16 SiO_2 layers and 15 Si layers were deposited alternately on ⟨100⟩ silicon substrates at the same temperature of 725 °C for both the Si and SiO_2 layers. In this case, the Si and SiO_2 layers were deposited continuously. For the deposition of Si layers, silane (SiH_4) was used as source gas; while for the deposition of SiO_2 layers, a gas mixture of silane and nitrous oxide (SiH_4+N_2O) was used with a ratio of the gas partial pressure ($Ro=N_2O/SiH_4$) of 100. Under this condition, the stoichiometric SiO_2 deposition was obtained.[14,15] By turning the valve on and off in the N_2O gas feeding line, the reactive

[a]Author to whom correspondence should be addressed; FAX: +52-222-2470517; electronic mails: zyu@inaoep.mx and yinaoep@yahoo.com

TABLE I. List of SL samples and corresponding thicknesses of the Si and SiO_2 layers. The *xC* and *xD* represent the samples at the as-deposited and annealed states, respectively.

Samples	SiO_2 thickness (nm)	Si thickness (nm)
1*C*/1*D*	0.92	5.0
3*C*/3*D*	2.7	5.0
5*C*/5*D*	5.0	5.0
7*C*/7*D*	2.7	2.5
9*C*/9*D*	2.7	8.0

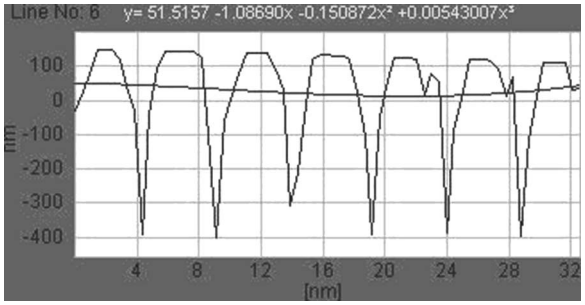

FIG. 1. An AFM one-dimensional scanning profile of the SL sample 7*D*. The observed valleys correspond to the etched oxide layers.

gases in the deposition chamber were controlled. As a result, the Si and SiO_2 layers were deposited alternately. The partial pressure of SiH_4 was optimized to obtain low deposition rates of 1.6 and 1.38 nm/min for Si and SiO_2, respectively. The first layer was always SiO_2, after that the Si layer was deposited by turning off the N_2O gas valve. Because the N_2O in the chamber cannot be instantly depleted, the Si layers were contaminated with O, and the interfaces possibly contain Si clusters surrounded by silicon oxide instead of a continuous Si layers. If the Si layers are too thin, the residual N_2O could affect the whole Si layers. In this study, five depositions were made. The thicknesses of the Si and SiO_2 layers were varied between 0.9 and 8.0 nm for the five samples as listed in Table I. After deposition, the samples were cut into two pieces. One-half of each sample was thermally annealed at 1100 °C in N_2 ambient for 2 h.

The structural properties of the SL films were studied using an atomic force microscopy (AFM, easyScan DFM, nanoSurf). The AFM specimen was made by sticking two SLs films face to face and then slicing it perpendicular to the layers. The sliced specimen was polished on one side of the sliced cross section. Then the polished specimen was dipped in a buffered HF solution, where the SiO_2 layers were partially etched. AFM images and line scan were taken on the etched cross section of the specimen.

Fourier transformed infrared (FTIR, Brucker FTIR spectrometer model V22) measurements were carried out to study the bonding configurations of the SLs films in a wave number range of 350–4000 cm^{-1} and with a step of 5 cm^{-1}. X-ray diffraction (XRD) measurements were carried out for crystalline structure analysis using a Rigaku MAX diffractometer operated at 40 kV and 100 mA. Cu $K\alpha_1$ ($\lambda = 0.154$ nm) line was used. The scanning region of 2θ was 10–90° with a step of 0.05°. The room-temperature PL spectra were measured for light-emission study using a spectrofluorometer (Fluoromax-3) with an excitation wavelength of 250 nm (4.96 eV). A 250 nm short-pass filter in the incident optical path and a 300 nm long-pass filter in the output optical path were used. The emission light was collected in the wavelength region of 300–900 nm.

III. RESULTS AND DISCUSSION

Figure 1 shows a one-dimensional scanning trace of sample 7*D*. A periodical structure with a period of ~5 nm is observed, which is close to the nominal period of 5.2 nm. The valleys in Fig. 1 correspond to the etched SiO_2 layers. In order to have a reliable measurement, we made several measurements with different scanning speeds and obtained the similar results as shown in Fig. 1. Therefore, the AFM measurements confirm that a layered structure was deposited using LPCVD. A cross-section transmission electron microscopic study is necessary to further confirm this result.

Figures 2(a) and 2(b) show the FTIR spectra of the SL samples at the as-deposited and annealed states, respectively. As a reference, an FTIR spectrum of a thermal SiO_2 film is shown in Fig. 2(c). The insets of Figs. 2(a) and 2(b) show typical FTIR spectra in a wide range from 300 to 2500 cm^{-1} (samples 3*C* and 3*D*, respectively), where eight emission peaks appear at both the as-deposited and annealed states. Table II summarizes the peak positions of the eight vibration modes and their identifications cited from the literature.[16–21] Peaks 1, 5, 6, and 7 (~450, ~810, ~1070, and ~1200 cm^{-1}) are attributed to the rocking, bending, symmetric stretching, and asymmetric stretching vibration modes of Si–O bond, respectively. Peak 2 (~550 cm^{-1}) is from interstitial oxygen. Peaks 3 and 4 (~612 and ~733 cm^{-1}) are attributed to Si–Si bond vibration modes with two different forms of oxygen vacancy, respectively. The oxygen vacancies may be formed either at the Si/SiO_2 interfaces or in the SiO_2 layers. The peak at 2350 cm^{-1} (peak 8) is supposed to be from $Si-H_x$ bond vibration as normally observed in hydrogenated amorphous silicon. Although the intensity is somewhat reduced, this peak is surprisingly still observable even after 1100 °C annealing in N_2. Therefore, the identification of peak 8 at the annealed state needs further investigation. The characteristic of the Si–O–Si stretching vibration mode (peak 6) is of particular interest for this study. Table III lists the maximum absorbance, peak position, and full width at half maximum (FWHM) of peak 6 of the five SL samples before and after annealing along with a SiO_2 bulk sample. From Table III, the following results are summarized

(1) The maximum absorbance of this peak increases with the increase of the SiO_2-layer thickness as observed in samples 1, 3, and 5. When the SiO_2 layer thickness is the same, the maximum absorbance increases with the increase of Si layer thickness (samples 7, 3, and 9). For a given sample, the thermal annealing increases maximum absorbance.
(2) The frequency (peak position) of this peak does not depend on the Si and SiO_2 layer thicknesses at both the as-deposited and annealed states. However, the thermal

annealing shifts this peak position from ~1063 to ~1080 cm^{-1}.

(3) The FWHM of this peak decreases after thermal annealing. In addition, the FWHM increases with SiO_2 layer thickness at both the as-deposited and annealed states.

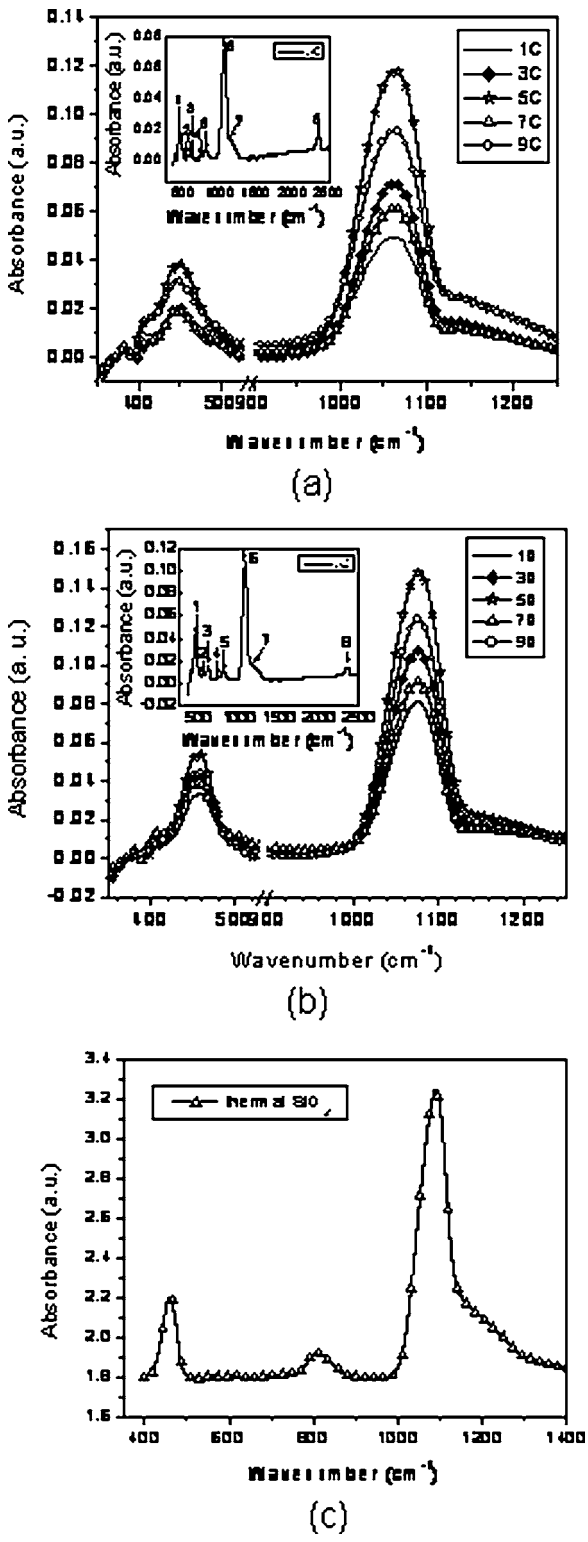

FIG. 2. FTIR Spectra of the SL samples at the as-deposited (a) and annealed (b) states. The insets in (a) and (b) show the identification of the eight absorption peaks. The plot (c) shows the absorption spectrum of a thermal SiO_2 sample.

TABLE II. Infrared vibration modes observed in the Si/SiO_2 SL samples.

Vibration mode	References	Wave number (cm^{-1}) Before annealing	Wave number (cm^{-1}) After annealing
(1) Si–O rocking	16, 17	447.4	457
(2) Interstitial Oxygen	21	547	550
(3) Si–Si (Oxygen's Vacancies)	21	612	612
(4) Si–Si (Oxygen's Vacancies)	21	733	736
(5) Si–O bending	16, 17, 18	811.5	810
(6) Si–O–Si stretching	16, 17, 18	1063	1080
(7) Si–O asymmetric stretching	16, 17, 18	1140	1250
(8) Si–H_x stretching	19, 20	2350	2350

The increase of the absorbance with the increase of the SiO_2 layer thickness is understandable because this peak is from the stretching mode of Si–O–Si bond. The increase of the SiO_2 layer thickness results in an increase in the average Si–O–Si bond density. However, the increase in the absorbance with the increase of the Si layer thickness for the same SiO_2 layer thickness remains a challenge for us to understand. One possible explanation is based on the assumption that the Si layers are in fact Si nanodots embedded in oxide matrix. In this case, the Si layers also have some contributions to this absorption peak, and therefore, the absorbance will increase with Si layer thickness.

The shift of the peak position to higher frequency and the decrease of FWHM after thermal annealing are due to the densification of the oxides (including the oxide phase in the Si layers). The peak position shifts to 1080 cm^{-1}, approaching to the corresponding absorption peak of thermal SiO_2 (1086 cm^{-1}). This indicates that the oxide phase in our SLs have almost the stoichiometric structure after annealing, which probably results from the phase separation from a silicon-rich oxide into the stoichiometric oxide and Si clusters or dots during the annealing process.

The FWHM of the Si–O–Si stretching vibration of the thermal stoichiometric SiO_2 is about 80 cm^{-1}. However, as

TABLE III. Lists of the maximum absorbance, peak position, and full-width-half-maximum (FWHM) of the stretching vibration peak of the SL samples. The results of the thermal oxide are also listed in the table for reference.

Sample	Peak position (cm^{-1}) *C* (before anneal)	Peak position (cm^{-1}) *D* (after anneal)	Peak intensity (a.u.) *C* (before anneal)	Peak intensity (a.u.) *D* (after anneal)	FWHM (cm^{-1}) *C* (before anneal)	FWHM (cm^{-1}) *D* (after anneal)
1	1063	1080	0.050	0.081	75	65
3	1063	1080	0.072	0.108	79.5	67.9
5	1063	1080	0.118	0.148	81	70.4
7	1063	1080	0.061	0.092	75.1	66.1
3	1063	1080	0.072	0.108	79.5	67.9
9	1063	1080	0.094	0.124	81	69.8
SiO_2	1086		···		80	

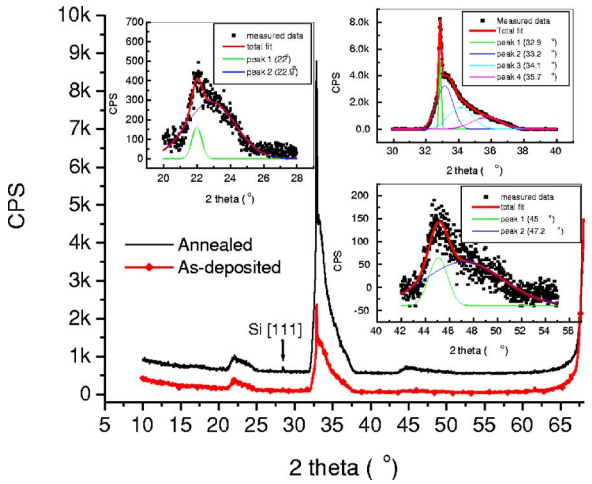

FIG. 3. (Color online) Typical XRD patterns of the SL samples. The three insets show the deconvolutions of the diffraction pattern around 22°, 33°, and 45°, respectively.

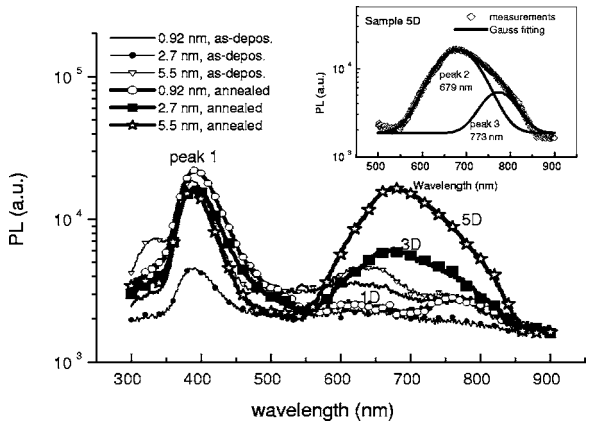

FIG. 4. The PL spectra of the SL samples with the same Si layer thickness of 5 nm, but with different SiO_2 layer thicknesses. The inset shows the deconvolution of the emission band of the sample *5D* in the range from 550 to 850 nm.

shown in Table III, our SL films show a FWHM smaller than 80 cm^{-1} except for samples 5 and 9 at the as deposited state. This result implies that the oxide layers in our SLs have a more ordered structure than that of the thermal SiO_2, especially after annealing. Furthermore, the increase of the FWHM with oxide layer thickness suggests that the ordering in the oxide layer is inhomogeneous along the layer thickness. The region near the Si/SiO_2 interfaces should have a smaller FWHM than that in the center of SiO_2 layers. From the result of FWHM <80 cm^{-1} and its variation with oxide thickness, we conclude that a very thin SiO_2 layer near each Si/SiO_2 interface has a very small distribution of Si–O–Si bonding angle. In other words, this thin SiO_2 layer near the interface is more ordered than the thermal SiO_2. In fact, Cho *et al.* have reported the formation of crystalline SiO_2 over very thin (<3 nm) Si layers.[22] Therefore, we propose that in our SL films, the SiO_2 layers are partially crystallized near the Si/SiO_2 interfaces, especially at the annealed state.

Figure 3 shows the typical XRD patterns of SL samples, where the three insets show the deconvolutions of the diffraction peaks at around 22°, 33°, and 45°. The very weak peaks at ~28° and 47.2° are attributed to the diffractions from [111] and [220] planes of crystalline Si, respectively. These two peaks are very weak, indicating a very small crystallite size or a very large amorphous volume fraction in the Si layers even after the thermal annealing at 1100 °C. It has been reported that the crystallization temperature increases with decreasing the Si thickness.[23] Therefore, the annealing at 1100 °C for 2 h is not long enough for fully crystallizing the thin Si layers in the SL samples. Other diffraction peaks at 22° and 35.7° can be attributed to the α and β cristobalite, respectively.[24] This result is consistent with the FTIR results that a certain crystalline SiO_2 phase is formed in the SL samples at the Si/SiO_2 interfaces. The thermal annealing enhances the diffraction intensity as shown in Fig. 3, which support the conclusion that crystalline SiO_2 layers formed during the thermal annealing. The strong diffraction peak can be deconvoluted into four peaks at 32.9°, 33.2°, 34.1°, and 45°, which is probably due to an unknown crystalline silicon oxide phase. The peak starting to increase near 67.5° of Fig. 3 is from the Si ⟨100⟩ substrate (this peak centers at 70°).

Figure 4 shows the PL spectra of the SL samples with the same Si layer thickness of 5.0 nm but with different SiO_2 layer thicknesses. The inset in Fig. 4 shows the deconvolution of the broad emission band in the range between 550 and 850 nm of sample *5D*. This emission band can be deconvoluted into two emission peaks. Thus a total of three emission peaks are observed in all the SL samples. The similar spectra were also observed in the SL samples with the same SiO_2 layer thickness of 2.7 nm but with different Si layer thicknesses as shown in Fig. 5. Peak 1 at 390 nm (3.2 eV) does not show a clear shift in peak position with the change of the Si or SiO_2 layer thickness. In addition, the intensity increases after annealing at the high temperature, but the changes are not as significant as peaks 2 and 3. As shown in Figs. 4 and 5, the intensities of peaks 2 and 3 are greatly enhanced after the thermal annealing, and their peak positions also shift to lower energies. We believe that the annealing enhanced PL intensity is due to the passivation of nonradiative defect states as well as the formation and growth of well-defined Si nanodots. Moreover, peaks 2 and 3 in Fig. 5 also show a clear redshift with increasing Si layer

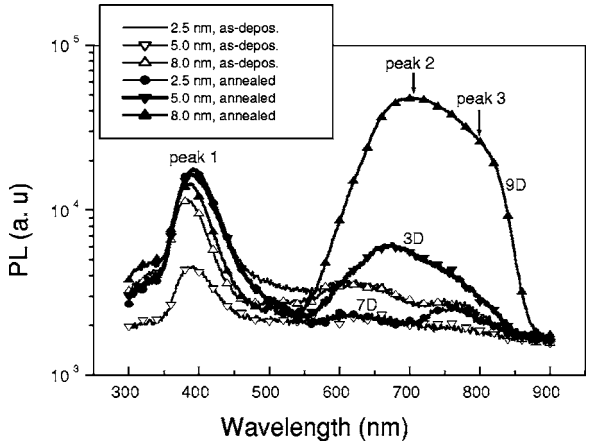

FIG. 5. The PL spectra of the SL samples with the same SiO_2 thickness of 2.7 nm, but with different Si layer thicknesses.

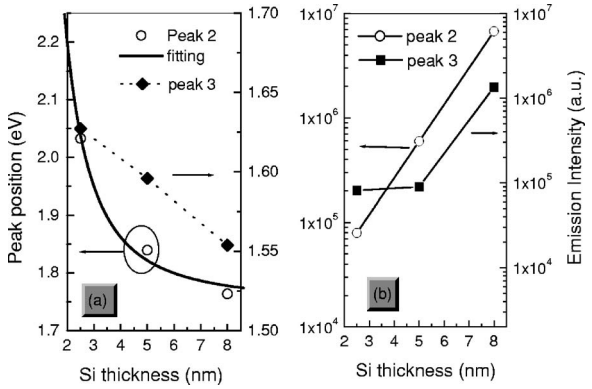

FIG. 6. The peak position and intensity of peaks 2 and 3 from Fig. 5 as functions of nominal Si layer thickness at the annealed state. The SiO_2 layer thickness remains constant at 2.7 nm.

thickness. But they show a little change with SiO_2 layer thickness as shown in Fig. 4, except for the case of the thinnest SiO_2 layer thickness (0.92 nm).

Peak 1 cannot be attributed directly to either the Si or SiO_2 layers, because it does not show clear layer-thickness dependence. Furthermore, the Si layers do not have such a large optical band gap even supposing that Si nanodots are of the same size of the layer thickness. The weak dependence of its position and intensity on the thermal annealing also supports this argument, because the thermal annealing modifies the microstructure of both the Si and SiO_2 layers as revealed by FTIR. The most possible origin of this peak is the recombination at the interfaces between Si and SiO_2 layers, where a large number of Si dangling bonds or other defects can contribute to the high energy PL. A similar emission peak was also observed in silicon-rich oxide deposited using PECVD and this peak also did not change after thermal annealing.[25]

Figure 6 shows the position and intensity of peaks 2 and 3 as a function of nominal Si layer thickness in the SL samples at the annealed state, where the SiO_2 layer thicknesses are the same at 2.7 nm. The emission peak 2 shifts from 1.76 to 2.05 eV when the Si layer thickness is varied from 8 to 2.5 nm. Peak 3 also shows a small shift from 1.55 to 1.63 eV. Because their positions do not clearly depend on the SiO_2 layer thickness, these peaks should be attributed to the Si layers. The solid line in Fig. 6(a) is a fit for the position of peak 2 using the theory of quantum confinement effect, which gives the equation of

$$E(\mathrm{eV}) = E_g + C/d^2, \tag{1}$$

where E is the peak energy, d is the nominal Si layer thickness (in nanometers), C is the confinement parameter, and E_g is the fitted band gap of the bulk Si. The best fit for the experimental data with Eq. (1) yields $C=1.8$ eV nm^2 and $E_g=1.75$ eV. The value of E_g is much larger than that of bulk c-Si (1.12 eV), but it is closer to the band gap of amorphous Si (1.5–1.9 eV). This means that the Si layer is in amorphous phase, which is consistent with XRD results where no clear silicon Bragg diffraction patterns are detected. The confinement parameter in this work are larger than that of the reported data obtained in the continuous Si quantum wells,[9] possibly due to the three-dimensional instead of one-dimensional confinement in our system.

According to the theory of quantum confinement effect, the PL intensity should be decreased as Si layer thickness increases.[9,10] However, our results show a contrary tendency as depicted in Fig. 6(b), where the PL intensity increases with Si layer thickness. This result can be explained by the increase of the density of luminescence centers, namely, Si nanodots, with the increase of the Si layer thickness.

Peak 3 cannot be explained by the theory of quantum confinement effect since its shift in peak position with Si layer thickness is smaller than the theoretical expectation. Because this peak is much weaker than peak 2, we suspect this emission could be from the radiative emission via the defects at the Si nanodots surface. These defects are normally located in the band gap of the Si nanodots, and their energy levels do not strongly depend on the size of the nanodots. The studies of the PL properties of Si nanocrystals (nc-Si) in SiO_2 show similar behavior,[1] where the position of PL due to the nc-Si/SiO_2 interfaces did not depend on the nc-Si size. With increasing the nominal Si layer thickness, the density of the Si nanodots increases, and consequently the density of defect states also increases. As a result the PL intensity of peak 3 increases with the increase of the Si layer thickness.

The PL peaks 2 and 3 observed in this study are consistent with the previous observations in the literature with two emission peaks in crystalline-Si/SiO_2 superlattices.[26,27] One strong PL peak from the recombination through the interface defects varies only from 1.65 to 1.80 eV, and a weak one from the quantum confinement effect varies from 1.50 to 2.30 eV, depending on the Si layer thickness. However, in our study, the PL emission from the quantum confinement effect is much stronger than that from the defects, which is possibly due to the stronger three-dimensional quantum confinement effect in our partially crystallized Si/SiO_2 SL films than the one-dimensional quantum confinement effect as reported in the literature.

IV. CONCLUSION

We have made Si/SiO_2 superlattices structures using LPCVD and studied their structural and optical properties using AFM, FTIR, XRD, and room-temperature PL measurements. Our results prove that the Si/SiO_2 layered structure can be deposited with the layers of Si nanodots embedded between SiO_2 layers by LPCVD. We find that the SiO_2 layers near the Si-layer interfaces are more ordered than the amorphous thermal SiO_2. The deposited SLs samples show an intensive PL at room temperature. Three PL peaks were observed: a high energy peak is from the recombination through the Si/SiO_2 interface states, a main emission peak at the middle energy region can be explained using the theory of quantum confinement effect in Si nanodots, and a weak peak is from the recombination through the defect states at the surface of Si nanodots.

ACKNOWLEDGMENTS

We would like to thank the financial supports from the NSF of China under Contract No. 50172061, CONACYT-SEP, and CONCYTEP-Fomix, Mexico. One of the authors (Z.Y.) appreciates Dr. B. Yan at United Solar Ovonic Corporation for his critical reading and valuable suggestions. The technical help in the preparation of the samples from Tania Calderón Medina, Pablo Alarcon, and Georgina Rosa is appreciated.

[1]T. Shimizu-Iwayama, D. E. Hole, and I. W. Boyd, J. Phys.: Condens. Matter **11**, 6595 (1999).
[2]K. S. Seol, Y. Ohki, H. Nishikawa, M. Takiyama, and Y. Hama, J. Appl. Phys. **80**, 6444 (1996).
[3]A. J. Kenyon, P. F. Trwoga, C. W. Pitt, and G. Rehm, J. Appl. Phys. **79**, 9291 (1996).
[4]F. Iacona, G. Franzo, and C. Spinella, J. Appl. Phys. **87**, 1295 (2000).
[5]L. Wu and F. S. Xue, Appl. Phys. Lett. **84**, 2807 (2004).
[6]D. J. DiMaria *et al.*, J. Appl. Phys. **56**, 401 (1984).
[7]J. F. Flores, M. Aceves, J. Carrillo, C. Domínguez, C. Falcony, and W. Calleja, Mod. Phys. Lett. B **15**, 704 (2001).
[8]T. Kim, N. Park, K. Kim, G. Sung, Y. Ok, T. Seong, and C. Choi, Appl. Phys. Lett. **85**, 5355 (2004).
[9]D. J. Lockwood, Z. H. Lu, and J.-M. Baribeau, Phys. Rev. Lett. **76**, 539 (1995).
[10]E.-C. Cho, M. A. Green, J. Xia, R. Corkish, P. Reece, and M. Gal, Appl. Phys. Lett. **84**, 2286 (2004).
[11]L. Tsybeskov, G. F. Grom, P. M. Fauchet, J. P. McCaffrey, J. M. Baribeau, G. I. Sproule, and D. J. Lockwood, J. Appl. Phys. **75**, 2265 (1999).
[12]G. F. Grom *et al.*, Nature (London) **407**, 358 (2000).
[13]L. Tsybeskov, K. D. Hirschman, S. P. Duttagupta, M. Zacharias, M. Fauchet, J. P. McCaffrey, and D. J. Lockwood, Appl. Phys. Lett. **72**, 43 (1998).
[14]D. Dong, E. A. Irene, and D. R. Young, J. Electrochem. Soc. **125**, 819 (1978).
[15]W. Calleja, C. Falcony, A. Torres, M. Aceves, and R. Osorio, Thin Solid Films **270**, 114 (1995).
[16]P. G. Pai, S. S. Chao, Y. Takagi, and G. Lucobesky, J. Vac. Sci. Technol. A **4**, 689 (1986).
[17]F. Ay and A. Aydinli, Opt. Mater. (Amsterdam, Neth.) **26**, 33 (2004).
[18]I. Pereyra and M. Alayo, Thin Solid Films **402**, 154 (2002).
[19]A. J. Kenyon, P. F. Trwoga, C. W. Pitt, and G. Rehm, J. Appl. Phys. **79**, 9291 (1996).
[20]M. Chayani, H. Caquineau, B. Despax, J. Bandet, and R. Berjoan, Thin Solid Films **471**, 53 (2005).
[21]T. Morioka, S. Kimura, N. Tsuda, C. Taito, Y. Saito, and C. Koike, Mon. Not. R. Astron. Soc. **299**, 78 (1998).
[22]E. C. Cho, M. A. Green, J. Xia, and R. Corkish, J. Appl. Phys. **96**, 3211 (2004).
[23]M. Zacharias, J. Bläsing, P. Veit, L. Tsybeskvo, K. Hirschman, and P. M. Fauchet, Appl. Phys. Lett. **74**, 2614 (1999).
[24]H. An, Y. Tang, P. McNamara, and S. Fleming, Opt. Express **12**, 1055 (2004).
[25]S. Dusane, T. Bhave, S. Hullavard, S. V. Bhoraskar, and S. Lokhare, Solid State Commun. **111**, 431 (1999).
[26]Y. Kanemitsu and S. Okamoto, Phys. Rev. B **56**, R15561 (1997).
[27]D. J. Lockwood, M. W. C. Dharma-wardana, Z. H. Lu, D. H. Grozea, P. Carrier, and L. J. Lewis, Mater. Res. Soc. Symp. Proc. **737**, F.1.1.1. (2003).